Original

Paula, A.S.; Mahesh, K.K.; Schell, N.; Braz Fernandes, F.M.:

Textural Modifications during Recovery in Ti-Rich Ni-Ti Shape Memory Alloy Subjected to Low Level of Cold Work Reduction

Materials Science Forum, Advanced Materials Forum V (2010)
Trans Tech Publications

DOI: 10.4028/www.scientific.net/MSF.636-637.618

Materials Science Forum Vols. 636-637 (2010) pp 618-623
Online available since 2010/Jan/12 at www.scientific.net

doi:10.4028/www.scientific.net/MSF.636-637.618

Textural Modifications during Recovery in Ti-Rich Ni-Ti Shape Memory Alloy Subjected to Low Level of Cold Work Reduction

A.S. Paula[1,2,a], K.K. Mahesh[3,b], N. Schell[4,c] and F.M. Braz Fernandes[3,d]

[1] CSN – GGDP/GPD, Rod. BR 393, km 5001 – Lúcio Meira, s/n – Vila Santa Cecília Volta Redonda – RJ – Brazil – CEP 27260-390

[2] UNIFoa – Centro Universitário de Volta Redonda, Campus Três Poços – Av. Paulo Erlei Alves Abrantes, 1325, Três Poços – Volta Redonda – RJ – Brazil – CEP 27240-560

[3] CENIMAT – I3N, Campus da FCT/UNL, 2829-516 Monte de Caparica, Portugal

[4] GKSS Research Center Geesthacht, Max-Planck-Str. 1, 21502 Geesthacht, Germany

[a] andersan.paula@csn.com.br, [a] andersita@yahoo.com.br, [b] kkm@fct.unl.pt, [c] norbert.schell@gkss.de, [d] fbf@fct.unl.pt

Keywords: Nitinol, Texture, Cold work, Recovery.

Abstract. In shape memory alloys (SMA), the texture can be an interesting factor influencing the anisotropic physical and mechanical characteristics during the phase transformations. It is well known that the texture significantly influences the stress-strain curve and shape memory strain of NiTi SMA. The aim of the present experiment was to analyze the textural modifications in the Ti-rich Ni-Ti SMA after annealing at moderate (500ºC for 30 min) and subsequent low level of cold work reduction (10% thickness reduction). The textural results were obtained by X-Ray Diffraction (XRD) during thermal cycling in three points: (i) at room temperature (B19' phase, after cold work), (ii) at 180ºC (B2 phase), and (iii) at room temperature (B19' phase, after cooling from 180ºC). The phase transformations were characterized by Differential Scanning Calorimetry (DSC) and XRD.

Introduction

Ni-Ti is a shape memory alloy with an equiatomic composition and is capable of two successive athermal martensitic phase transformations while cooling from its higher temperature austenite (B2 – CsCl crystal structure) phase. In Ti-rich Ni-Ti SMA, the first phase transformation during cooling is observed above room temperature and results in the R-phase (trigonal crystal structure with rhombohedral distortion in angle α); the second one occurs around room temperature and results in M-phase (B19' – monoclinic structure), often with a fine lath morphology. These transformations give rise to thermoelasticity and twin deformations in Ni-Ti alloy facilitating shape memory effect (SME) [1].

Ni-Ti SMA is highly ductile, compared with other intermetallic compounds, and, when subjected to tensile loading, elongations above 20% are commonly reported [2-4]. Yet, in the martensitic condition, these alloys possess a low symmetry B19' monoclinic crystal structure, which might restrict dislocation movement to some extent. In contrast, significant dislocation activity has been reported in the alloys deformed in tensile/compression mode, where dislocation generation and their pile-ups at the twin boundaries have been observed [4,5].

Several studies are dedicated to the influence of the texture on thermomechanical response of the SMAs [6-15]. Thermal cycling, rolling or drawing are found to develop specific texture in metals and alloys. They result in different anisotropy characteristics (mechanical, electrical and magnetic behavior). NiTi SMAs are also sensitive to these effects. The texture is found to give rise to anisotropy in transformation recovery strain [10]. NiTi SMA in austenitic field has a bcc type texture [11,12]: α-fiber I <110>||RD ({001}<112>-{112}<110>-{111}<110>), α-fiber II <110>||RD ({111}<110>-{110}<110>), γ fiber <111>||ND ({111}<110>-{111}<112>), and η-fiber <100>||RD

({001}<100>-{011}<100>). The calculated lattice correspondence between parent phase and martensite using the notation of the correspondence variant from Miyazaki [6], where {110}<1 $\bar{1}$ 0> parent phase variant correspond to {111}<211> and {002}<002> martensite variants; and {111}<1 0> parent phase correspond to {210}<211> and {210}<002>.

The recovery and recrystallization terms are attributed to the process that are different of those usually applied to metal and alloys. After the cold work, the recovery term usually refers to dislocation reorganization inside the previous grains that lead to a dislocation structure (polygonization). The recrystallization occurs at much high temperatures by new grains nucleation and growing, stress relief, starting from points with high defects concentration, resulting in point defects elimination. The Ni-Ti SMA is more complicated [5]: the cold work is produced in the martensitic state and plastic deformation does not occur in the first austenite grains, but in the martensite variants with different crystallographic orientations. The plastic deformation includes primarily the martensite reorientation of martensite variants, and, only after that, the dislocation generation inside each martensite variant.

In the present work we investigated how low level cold work in Ni-Ti SMA can affect the SME and the modifications in crystallographic texture during recovery process at this deformation stage.

Experimental

The samples for the present study were extracted from straight annealed (as-received condition – AR) Ti-rich Ni-Ti alloy (Ni-51.0at%Ti) plate of thickness 2 mm supplied by Memory-Metalle GmbH, Germany. The samples were analyzed in the following conditions: (i) heat treated at 500ºC (HT) and (ii) heat treated at 500ºC followed by 10% thickness reduction by cold rolling (HT + CW10%). The heat treatment (HT) was performed by holding the specimen at 500ºC for 30 minutes and subsequently quenching in water at room temperature (T_{room}). The samples were subjected to chemical etching (10% vol HF + 45% vol HNO_3 + 45% vol H_2O) in order to remove the oxide layer as well as the layer deformed during the cutting operation.

Samples with a mass ranging from 40 to 50 mg were cut from all specimens for DSC analysis (SETARAM DSC92). The following thermal cycle was used for the DSC tests: start temperature at T_{room}, heating to 180ºC, holding for 360 s and subsequent cooling down to -30ºC, with heating and cooling rates of 7.5ºC/min (Fig. 1).

XRD analysis was performed using a Bruker diffractometer (rotating anode – XM18H, CuKα radiation, 30 kV/100 mA, D5000 goniometer) with conventional θ/2θ scannings at various temperatures between T_{room} and 180ºC (Fig. 2) , and texture analysis at T_{room} (B19' phase) and 180ºC (B2 phase) (Fig. 3 and 4). The rolling direction (RD) was kept aligned in φ = 0º, with the transversal direction (TD) in φ = 90º.

XRD analysis was performed at ROBL/BM20 of ESRF (Fig. 1a) for the in-situ high temperature θ/2θ scans. In-situ XRD analysis during annealing has been carried out using X-rays of wavelength 1.54 Å and a vacuum furnace with hemispherical Be-dome evacuated to a pressure less than $2x10^{-6}$ mbar. The furnace was installed on the ϕ circle (azimuthal orientation) of a six-circle goniometer. The rolling direction (RD) is aligned with ϕ = -55º. The structural evolution was observed by in situ XRD during annealing up to 400ºC for the samples in study (Fig. 5).

Results and Discussion

The Fig. 1 shows the DSC curves for HT and HT+CW10% samples. The transformation temperatures of the HT sample were not changed compared to the AR material. But the HT+CW10% sample shows some modifications: reduction of the peak areas and changes of the transformation temperatures. This reduction on the DSC peak areas is relate to the SME partial loss; the partially deformed martensite (reoriented and with dislocations) is not fully reverted austenite (Figure 5b) [9,10,16]. However the changes on direct and reverse transformation temperatures are

related to introduction of internal stress fields (associated to dislocations density on the Ni-Ti matrix) on the structure that increase the energy needed for B2↔B19' transformation to occur, stabilize the martensite (B19') and promote the R-phase intermediate transformation on heating and on cooling [17,18].

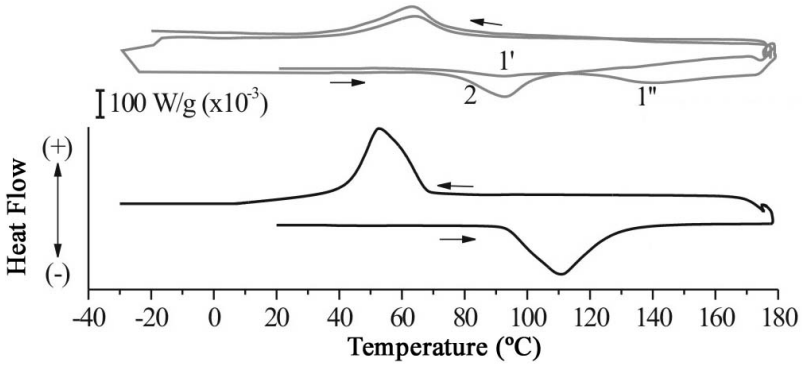

Fig. 1 – DSC Curves for HT (one cycle) and HT+CW10% (two cycles) samples.

Other evidences about the martensite plastic deformation are presented by XRD spectra (Fig. 2) and B19' texture (Fig. 3a and 4a) for HT and HT+CW10% samples in martensitic state at room temperature.

The XRD spectra (Fig. 2) exhibits an evolution of relative peak intensities, where the net area of the (021) martensite diffraction peak of the HT sample (deformation free) increases when compared to HT+CW10% (10% cold work). On the other hand, the other diffraction peaks net area ((101), (020), (111) and (002)) decrease.

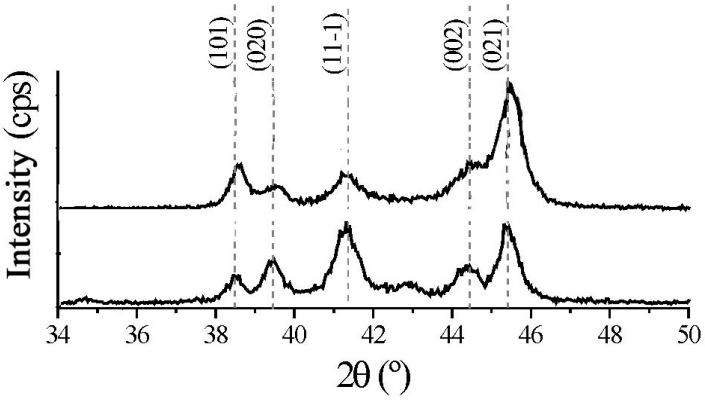

Fig. 2 – XRD Spectra for HT and HT+CW10% samples at room temperature.

The Fig. 3 shows the $(11\bar{1})_{B19'}$ and $(110)_{B2}$ pole figures for HT sample. The HT sample exhibits reinforcement close to central components (φ = 0º, χ = 0º) and close to χ = 30º. These reinforcements are associated to the following texture components:

(i) for the B19', near to the central variants $1{:}(11\bar{1})[2\bar{1}1]_{B19'}$ and $4{:}(11\bar{1})[\bar{2}1\bar{1}]_{B19'}$ related to $\{110\}\langle 110\rangle_{B2}$ near to the variants $3{:}(120)[\bar{2}11]_{B19'}$ and $5{:}(120)[00\bar{2}]_{B19'}$ with χ = 33º related to $\{111\}\langle 110\rangle_{B2}$;

(ii) for the B2, near to the central component $(110)[110]_{B2}$ and near to the components $\{111\}\langle 110\rangle_{B2}$ with χ = 35º, with <110> along RD.

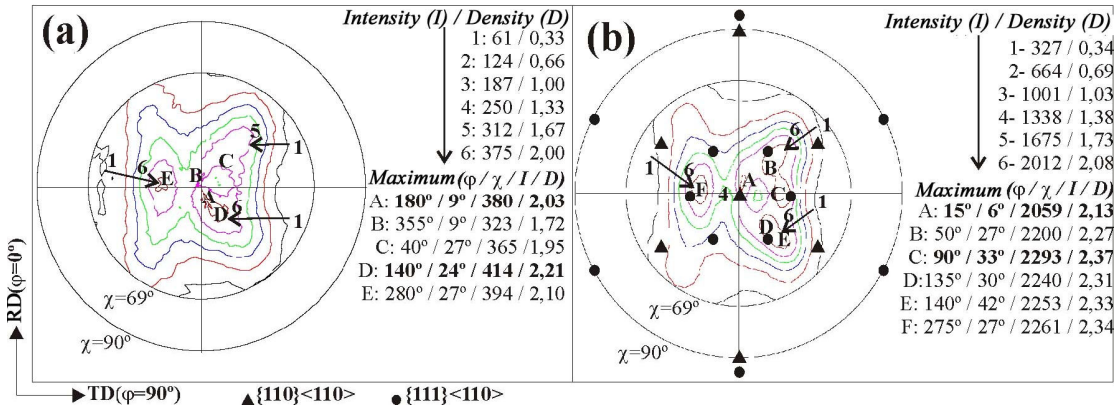

Fig. 3 – Pole Figures for HT Sample: (a) $(11\bar{1})_{B19'}$ and (b) $(110)_{B2}$.

The Fig. 4 present the pole figures for B19' before heating, B2 and B19' after heating for HT+CW10% sample; as shown in DSC curves (Fig.1), this sample, after heating above A_f (austenite final transformation temperature), exhibits a SME partial recovery. The HT+CW10% B19' pole figure reveals that the low level cold work is responsible for the reinforcement near $\chi = 30°$, associated to B19' texture components close to texture variants $3:(120)[\bar{2}11]_{B19'}$ and $5:(120)[00\bar{2}]_{B19'}$ related with $\{111\}\langle 110\rangle_{B2}$. The B2 pole figure for HT+CW10% sample (Fig. 4b) is totally different when compared with HT sample (Fig. 3b), showing a central reinforcement ($\varphi = 0°$, $\chi = 0°$) associated to the texture component $(110)[110]_{B2}$, plus a small contribution of the texture component $\{111\}\langle 110\rangle_{B2}$ close to $\chi = 35°$, <110> along DL. After heating, the B19' crystallographic texture changes: new secondary components appear near the variants $2:(10\bar{2})[211]_{B19'}$, $4:(10\bar{2})[\bar{2}1\bar{1}]_{B19'}$ and $6:(10\bar{2})[0\bar{2}0]_{B19'}$ associated to $\{111\}\langle 110\rangle_{B2}$; at the same time, decreases the relevance of the reinforcement near $\chi = 30°$, associated to B19' texture components close to texture variants $3:(120)[\bar{2}11]_{B19'}$ and $5:(120)[00\bar{2}]_{B19'}$ related with $\{111\}\langle 110\rangle_{B2}$.

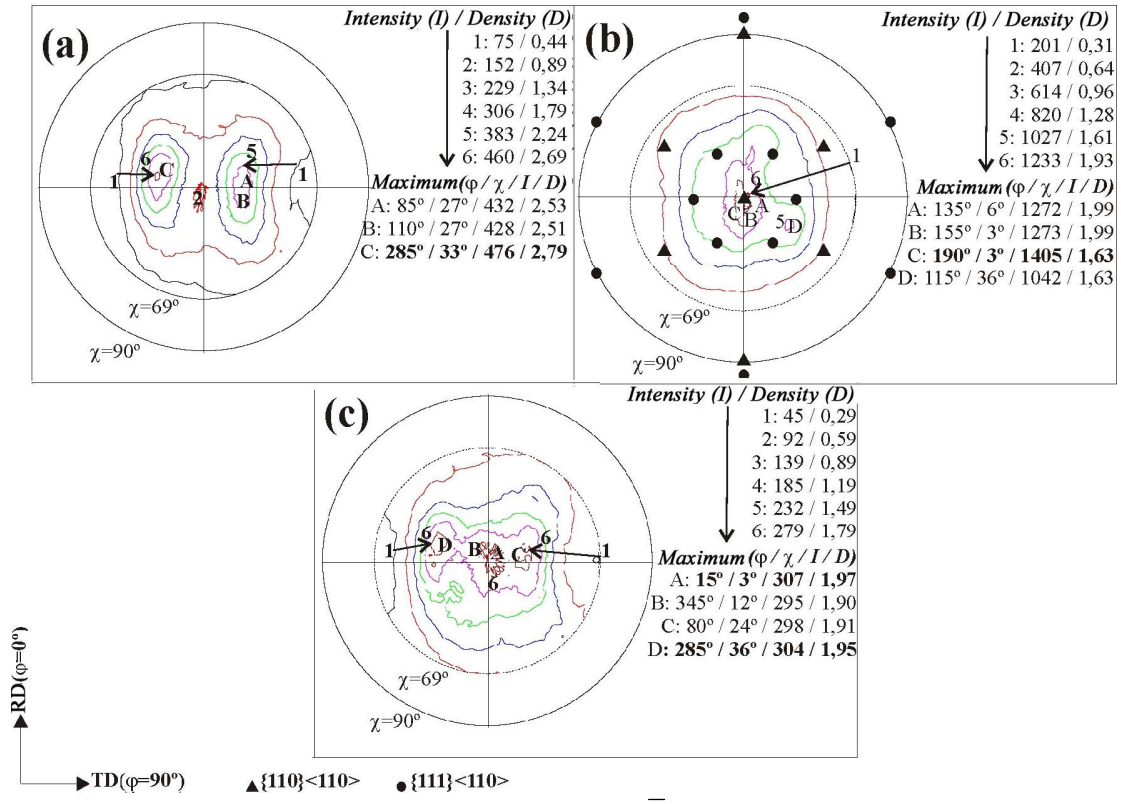

Fig. 4 – Pole Figures for HT+CW10% Sample: (a) $(11\bar{1})_{B19'}$ at T_{room} before heating, (b) $(110)_{B2}$, and (c) $(11\bar{1})_{B19'}$ at T_{room} after heating.

Figures 5a and 5b show the structural evolution differences between a deformation free martensitic sample (HT) and deformed martensitic sample (HT+CW10%) when submitted to a thermal cycle on heating up to 400ºC during in-situ XRD at high temperature on vacuum (ESRF). It is possible to verify that, when heating a deformation free sample (HT), the net area of the (110) austenite peak diffraction gradually increased (starting at 80ºC) as a result of the martensite consumption during B19'→B2 transformation on heating. On the other hand, if a martensitic sample with low deformation level (HT+CW10%) is heated , the XRD martensitic peak persists up to 130ºC and, only at this temperature, the intensity of the (110) austenite peak slowly increases. At 350ºC occurs an abrupt increase of the (110) austenite peak: the recrystallization starts at this temperature and finishes around 450ºC. The recovery and recrystallization behaviors are shown in Fig. 5c by the changes in the coherency domain size (CDS) and microstrain as a function of annealing temperature up to 400ºC for the HT+CW10% sample: (i) the CDS increases when the temperature increases, and (ii) the microstrain decreases with increasing temperature. The CDS values are related with the length of a "column" along which the interplanar distance is kept constant due to the absence of structural defects. In the case of HT+CW10%, previously submitted to 10% thickness reduction during cold working, the CDS is related to the deformation sub-cells. The non-uniform microstrain causes diffraction peak profile broadening. A very significant change in microstrain takes place above 200ºC up to 450ºC; instead, the CDS slowly increases up to 300ºC. According to other authors [9,10,16], this can be interpreted as an indication that recovery occurs below 200ºC, and recrystallization starts above 300ºC and finishes at 450ºC.

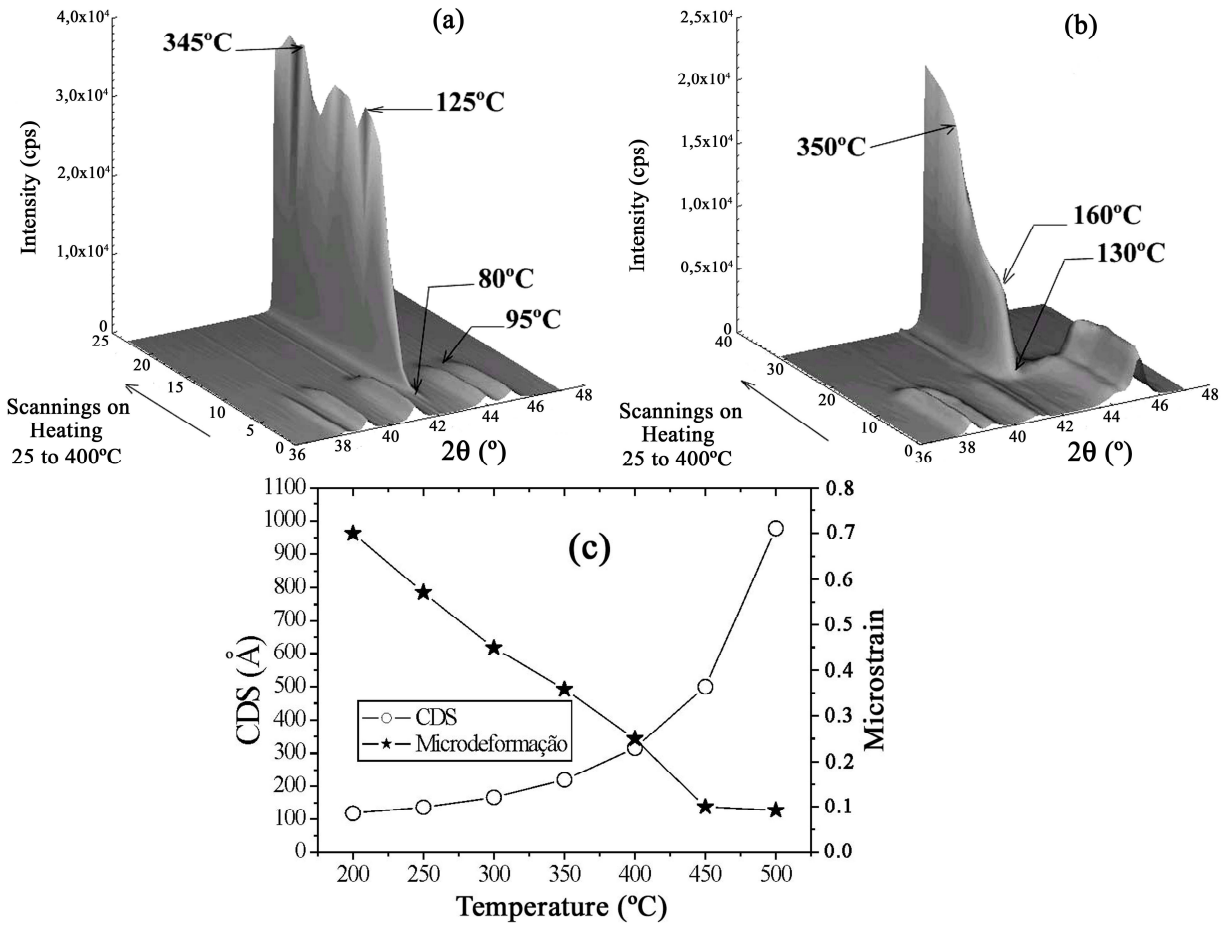

Fig. 5 – Structural evolution on heating (25 to 400ºC) during XRD in-situ at high temperature on vacuum (ESRF): (a) HT, and (b) HT+CW10%. (c) Changes on coherency domain size (CDS) and microstrain up to 400ºC, related to $(110)_{B2}$ XRD peak for HT+CW10% sample.

Summary

The low level of cold work (10% thickness reduction) of Ti-rich Ni-Ti shape memory alloy promotes SME partial loss when heated up to 150ºC (slightly above Af temperature) due to:
- increase in dislocation density on the martensitic matrix revealed by low values of CDS and high values of microstrain;
- recovery and recrystallization processes only promote changes in CDS and microstrain above 200ºC;
- permanent modification on the B19' and B2 crystallographic texture by introducing a secundary texture component associated to $\{111\}<110>_{B2}$ and variants 2:(102)$[211]_{B19'}$, 4:(102)$[211]_{B19'}$ and 6:(102)$[020]_{B19'}$, in parallel with the major component $\{110\}<110>_{B2}$ and variants 1:(111)$[211]_{B19'}$ and 4:(111)$[211]_{B19'}$, <332> along RD.

Acknowledgements

We would like to thank Dr. Rui M. S. Martins and Eng. Ana M. A. Cardoso for technical assistance and ESRF for financial support for the experiment 20_02_626 at ROBL. A.S.P. and F.M.B.F. acknowledge FCT/MCTES for the pluriannual financial support of CENIMAT/I3N.

References

[1] A.L. McKelvey, *et.al.*: Metallurgical and Materials Transactions 32A (2001), p. 731.

[2] K.N. Melton, *et.al.*: Acta Metallurgica 29 (1981), p. 393.

[3] K.N. Melton: Engineering Aspects of Shape Memory Alloys (Ed. Duerig T.W.), vol. 21, pp. 21-35, Butterworth-Heinemann, London, 1990, Editorial.

[4] H.F. Lopez, *et.al.*: Metallurgical and Materials Transactions A32 (2001), p. 717.

[5] Y. Liu, *et.al.*: Acta Materialia 47 (1999), p. 645.

[6] S. Miyazaki, *et.al.*: Acta Metall. Vol. 37 (1989), p. 1873.

[7] L. Zhao, Ph.D. thesis, University of Twente, Enschede, The Netherlands (1997).

[8] K. Kitamura, *et.al.*: SMST-97 (1997), p. 47.

[9] A.S. Paula, *et.al.*: NIM-B 238 (2005), p. 111.

[10] F.M. Braz Fernandes, *et.al.*: SMST2004 (2004), p. 45.

[11] T. Bhattacharya, *et.al.*: Acta Mater. Vol. 44-2 (1996), p. 529.

[12] Y.C. Shu, *et.al.*: Acta Mater. Vol. 46-15 (1998), p. 5457.

[13] A.S. Paula, *et.al.*: NIM-B 246 (2006), p. 206.

[14] A.S. Paula, *et.al.*: Materials Science Fórum, 495-497 (2005), p. 125.

[15] A.S. Paula, *et.al.*: 62th Annual ABM Congress – Vitória-ES / Brazil (2007), p. 3426.

[16] E. Hornbogen: Mater. Sci. Forum Vol. 455-456 (2004), p. 335.

[17] A.S. Paula, *et.al.*: Mat. Sci. and Eng. A Vol. 378 (2004), p. 92.

[18] F.M. Braz Fernandes, *et.al.*: SMST2004 (2004), p. 51.

Advanced Materials Forum V
doi:10.4028/www.scientific.net/MSF.636-637

Textural Modifications during Recovery in Ti-Rich Ni-Ti Shape Memory Alloy Subjected to Low Level of Cold Work Reduction
doi:10.4028/www.scientific.net/MSF.636-637.618

References

1] A.L. McKelvey, et al.: Metallurgical and Materials Transactions 32A (2001), p. 731.

[2] K.N. Melton, et al.: Acta Metallurgica 29 (1981), p. 393.
doi:10.1016/0001-6160(81)90165-6

[3] K.N. Melton: Engineering Aspects of Shape Memory Alloys (Ed. Duerig T.W.), vol. 21, pp. 21-35, Butterworth-Heinemann, London, 1990, Editorial.

[4] H.F. Lopez, et al.: Metallurgical and Materials Transactions A32 (2001), p. 717.

[5] Y. Liu, et al.: Acta Materialia 47 (1999), p. 645.
doi:10.1016/S1359-6454(98)00376-0

[6] S. Miyazaki, et al.: Acta Metall. Vol. 37 (1989), p. 1873.
doi:10.1016/0001-6160(89)90072-2

[7] L. Zhao, Ph.D. thesis, University of Twente, Enschede, The Netherlands (1997).

[8] K. Kitamura, et al.: SMST-97 (1997), p. 47.

[9] A.S. Paula, et al.: NIM-B 238 (2005), p. 111.
doi:10.1016/j.nimb.2005.06.028

[10] F.M. Braz Fernandes, et al.: SMST2004 (2004), p. 45.

[11] T. Bhattacharya, et al.: Acta Mater. Vol. 44-2 (1996), p. 529.

[12] Y.C. Shu, et al.: Acta Mater. Vol. 46-15 (1998), p. 5457.

[13] A.S. Paula, et al.: NIM-B 246 (2006), p. 206.
doi:10.1016/j.nimb.2005.12.029

[14] A.S. Paula, et al.: Materials Science Fórum, 495-497 (2005), p. 125.
doi:10.4028/www.scientific.net/MSF.495-497.125

[15] A.S. Paula, et al.: 62th Annual ABM Congress – Vitória-ES / Brazil (2007), p. 3426.

[16] E. Hornbogen: Mater. Sci. Forum Vol. 455-456 (2004), p. 335.

doi:10.4028/www.scientific.net/MSF.455-456.335

[17] A.S. Paula, et al.: Mat. Sci. and Eng. A Vol. 378 (2004), p. 92.
doi:10.1016/j.msea.2003.11.057

[18] F.M. Braz Fernandes, et al.: SMST2004 (2004), p. 51.